Geophysical Research Letters

RESEARCH LETTER
10.1029/2023GL105762

Key Points:

- Chemistry yields 4% and 20% ozone depletion in the lower stratosphere at mid-latitudes and Antarctica in August and October, respectively
- The majority of ozone depletion is ascribed to internal variability and dynamical changes induced by the eruption
- HTHH aerosol plume is associated with notable NO_x reduction, indicating enhanced dinitrogen pentoxide hydrolysis on sulfate aerosol

Supporting Information:

Supporting Information may be found in the online version of this article.

Correspondence to:

J. Zhang,
jzhan166@ucar.edu

Citation:

Zhang, J., Kinnison, D., Zhu, Y., Wang, X., Tilmes, S., Dube, K., & Randel, W. (2024). Chemistry contribution to stratospheric ozone depletion after the unprecedented water-rich Hunga Tonga eruption. *Geophysical Research Letters*, *51*, e2023GL105762. https://doi.org/10.1029/2023GL105762

Received 1 AUG 2023
Accepted 17 MAR 2024

Chemistry Contribution to Stratospheric Ozone Depletion After the Unprecedented Water-Rich Hunga Tonga Eruption

Jun Zhang[1], Douglas Kinnison[1], Yunqian Zhu[2,3], Xinyue Wang[4], Simone Tilmes[1], Kimberlee Dube[5], and William Randel[1]

[1]Atmospheric Chemistry Observations & Modeling Laboratory, National Center for Atmospheric Research, Boulder, CO, USA, [2]Cooperative Institute for Research in Environmental Sciences, University of Colorado Boulder, Boulder, CO, USA, [3]Chemical Sciences Laboratory, National Oceanic and Atmospheric Administration, Boulder, CO, USA, [4]Department of Atmospheric and Oceanic Sciences, University of Colorado Boulder, Boulder, CO, USA, [5]Institute of Space and Atmospheric Studies, University of Saskatchewan, Saskatoon, SK, Canada

Abstract Following the Hunga Tonga–Hunga Ha'apai (HTHH) eruption in January 2022, stratospheric ozone depletion was observed at Southern Hemisphere mid-latitudes and over Antarctica during the 2022 austral wintertime and springtime, respectively. The eruption injected sulfur dioxide and unprecedented amounts of water vapor into the stratosphere. This work examines the chemistry contribution of the volcanic materials to ozone depletion using chemistry-climate model simulations with nudged meteorology. Simulated 2022 ozone and nitrogen oxide ($NO_x = NO + NO_2$) anomalies show good agreement with satellite observations. We find that chemistry yields up to 4% ozone destruction at mid-latitudes near ~70 hPa in August and up to 20% ozone destruction over Antarctica near ~80 hPa in October. Most of the ozone depletion is attributed to internal variability and dynamical changes forced by the eruption. Both the modeling and observations show a significant NO_x reduction associated with the HTHH aerosol plume, indicating enhanced dinitrogen pentoxide hydrolysis on sulfate aerosol.

Plain Language Summary The January 2022 eruption of the Hunga Tonga-Hunga Ha'apai underwater volcano injected a large amount of water vapor (H_2O) and moderate amounts of sulfur dioxide (SO_2) into the stratosphere. Stratospheric ozone depletion was observed following the eruption at Southern Hemisphere (SH) mid-latitudes and over Antarctica during the 2022 austral wintertime and springtime, respectively. The ozone layer in the stratosphere protects both people and the biosphere by absorbing harmful solar ultraviolet radiation. We use computer simulation to examine the impacts of chemical processes on the ozone layer from the volcanic materials. We find that chemistry results in 4% and 20% of the ozone loss at SH mid-latitudes near 70 hPa in August and Antarctica around 80 hPa in October respectively. Most of the ozone changes are due to transport and dynamical processes from internal variability in the climate system and a forced response by the HTHH eruption.

1. Introduction

It has long been known that explosive volcanic eruptions can cause stratospheric ozone depletion by injecting sulfate and its precursor SO_2 into the stratosphere, which enhances aerosol surface areas for heterogeneous chemistry (Hofmann & Solomon, 1989; Kinnison et al., 1994; Portmann et al., 1996; Solomon et al., 1996, 1998). Observations have shown that Antarctic ozone depletion was enhanced after the major eruption of Mount Pinatubo in June 1991 with injections of ~18 Tg sulfur dioxide (SO_2) (e.g., Krueger et al., 1995; Read et al., 1993; Solomon et al., 2005). Even the moderate magnitude volcanic eruption of Calbuco (1.33°S, 287.39°E) in 2015, which injected 0.4 Tg of SO_2, exacerbated ozone depletion, producing a record-breaking October Antarctic ozone hole that lasted late into the season (Ivy et al., 2017; Solomon et al., 2016; Stone et al., 2017; Zhu et al., 2018).

The January 2022 Hunga Tonga–Hunga Ha'apai (HTHH) eruption (20.5°S, 175.4°W) was an unprecedented underwater volcanic event in the satellite era, injecting volcanic materials as high as 58 km above the Earth's surface (into the mesosphere) (Carr et al., 2022; Proud et al., 2022). Unlike land-based volcanoes such as Mount Pinatubo and Calbuco, HTHH injected about 150 Tg of water (H_2O) (Khaykin et al., 2022; Millan et al., 2022; Randel et al., 2023; Vömel et al., 2022) along with 0.4–0.5 Tg SO_2 into the stratosphere (Carn et al., 2022; Millan

et al., 2022; Taha et al., 2022). This H_2O injection increased the global stratospheric water burden by more than 10%. The additional source of H_2O can impact the ozone chemistry by altering the HO_x chemical cycles, heterogeneous reaction rates, and the Polar Stratospheric Cloud formation (Anderson et al., 2012; Solomon et al., 1997). In addition, volcanic aerosols provide extra surface area density (SAD) for heterogeneous reactions affecting ozone chemistry, suppressing the nitrogen oxide ozone depleting cycles (Tie & Brasseur, 1995).

Previous studies have utilized the Community Earth System Model Version 2 (CESM2) Whole Atmosphere Community Climate Model Version 6 (WACCM6) to simulate the dispersion and evolution of aerosol and water plumes after the HTHH eruption (Lu et al., 2023; Wang et al., 2023; Zhu et al., 2022). WACCM6 simulations reproduced the evolution of the H_2O throughout 2022 observed by the Microwave Limb Sounder (MLS) and the stratospheric cooling and circulation changes simulated by the European Center for Medium-Range Weather Forecasts (ECMWF) ERA5 reanalysis (Wang et al., 2023; Figure S1 in Supporting Information S1). The additional water vapor increases hydroxyl radicals, reduces the sulfur dioxide lifetime by 50%, and promotes faster sulfate aerosol formation, as seen by Cloud-Aerosol Lidar and Infrared Pathfinder Satellite Observation (CALIPSO) and the Ozone Mapping and Profiler Suite Limb Profiler (OMPS-LP), and leads to an increased aerosol optical depth (Kloss et al., 2022; Taha et al., 2022; Zhu et al., 2022). The persistent perturbations in H_2O and aerosol due to HTHH plumes in the Southern Hemisphere (SH) stratosphere throughout 2022 significantly altered the atmosphere, motivating a need to understand the SH stratospheric ozone response.

Manney et al. (2023) studied SH nitrous oxide (N_2O) anomalies, along with ozone anomalies, and suggested that transport plays a role in the observed ozone reduction. In this work, we aim to examine chemical ozone depletion and the associated chemical processes in the wake of HTHH. We isolate the ozone impact due to chemistry by nudging the model dynamics and temperature to meteorological reanalysis results. We note that by design the nudging method will not allow quantification of the potential dynamical feedback on chemistry as coupling between ozone loss and temperature is not considered.

2. Data and Model

2.1. Satellite Data

The data from MLS, Optical Spectrograph and InfraRed Imager System (OSIRIS) and OMPS-LP are utilized in this analysis. MLS Version 5.0 data is used in this work and the O_3 data and its validation are described by Livesey et al. (2020). Here the O_3 data used are daily zonal means with a horizontal resolution of 2.5°. MLS does not have high latitude measurements beyond 82°S due to the constraints of Aura Satellite orbit. OSIRIS has been in sun-synchronous orbit on the Odin satellite since 2001 (Llewellyn et al., 2004; Murtagh et al., 2002). In this study we use NO_x from version 7.2 of the OSIRIS retrieval, which is described and validated in Dubé et al. (2022). The OSIRIS NO_2 observations are converted to NO_x using the PRATMO photochemical box model (McLinden et al., 2000; Prather & Jaffe, 1990), following the process described in Dubé et al. (2020). Aerosol extinction data are from the University of Saskatchewan OMPS-LP product (Bourassa et al., 2023). These data, derived from a tomographic inversion, provide height-resolved aerosol extinction at 745 nm with a tomographic inversion, with a vertical resolution of 1–2 km.

2.2. Whole Atmosphere Community Climate Model (WACCM)

CESM2/WACCM6 was used to conduct the numerical experiments. This state-of-the-art chemistry-climate model extends from the Earth's surface to approximately 140 km and includes comprehensive troposphere-stratosphere-mesosphere-lower-thermosphere (TSMLT) chemistry (details described in Gettelman et al., 2019). WACCM6 includes a prognostic stratospheric aerosol module (Mills et al., 2016) and has been utilized extensively to study volcanic aerosols and their impact on climate change and ozone losses (e.g., Mills et al., 2017; Stone et al., 2017; Zambri et al., 2019). In this study, the simulations feature a horizontal resolution of 0.9° latitude × 1.25° longitude using the finite volume dynamical core (Lin & Rood, 1996), and 110 vertical levels, with a vertical resolution of ∼500 m in the upper troposphere and lower stratosphere. WACCM6 is run in a specified dynamics configuration (WACCM6-SD), where the temperatures and horizontal winds (U, V) are relaxed (i.e., nudged) to Modern-Era Retrospective analysis for Research and Applications Version 2 (MERRA-2) reanalysis (Gelaro et al., 2017) using a relaxation timescale of 12 hr. The nudging method used in this study follows the work of Davis et al. (2022). This configuration runs from 2007 until the end of 2022, using initial conditions from a long historical simulation (Gettelman et al., 2019). The model setup includes major

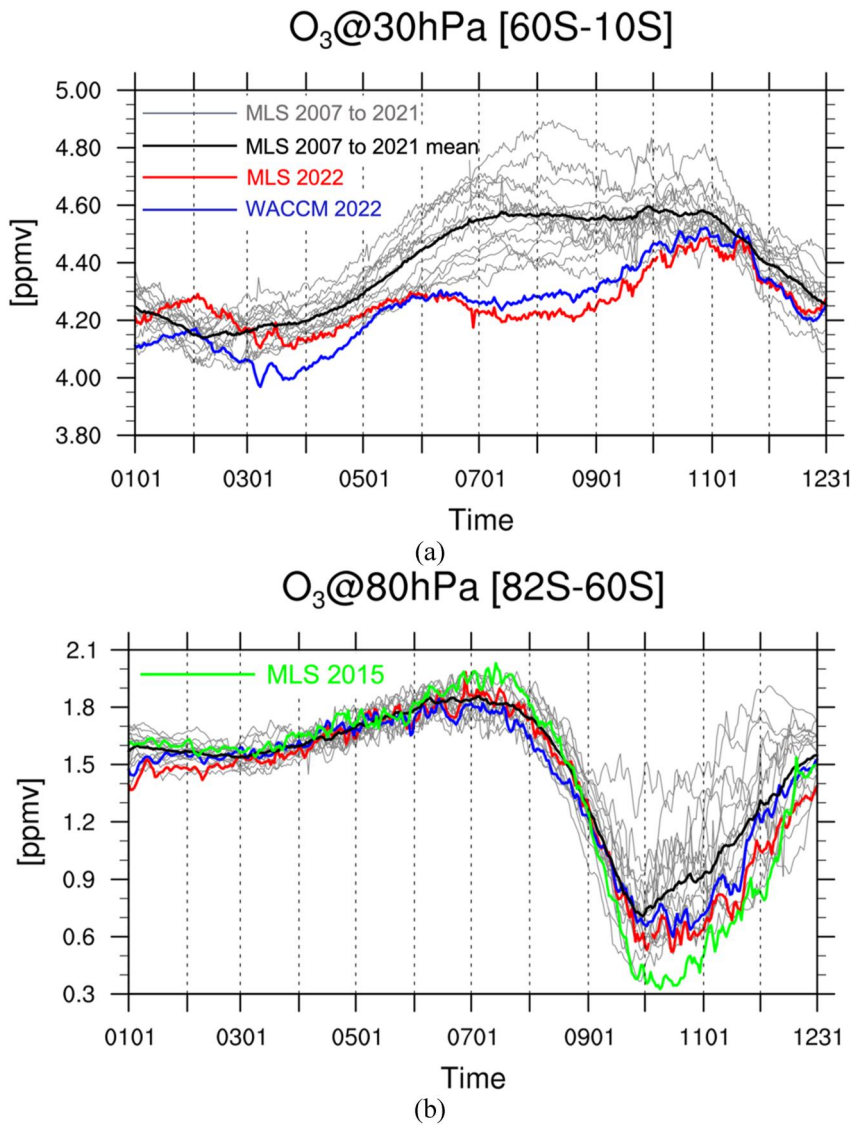

Figure 1. Time series of ozone concentration (ppmv) for (a) midlatitudes and tropics (10°S–60°S) at 30 hPa and (b) polar region (60°S–82°S) at 80 hPa from Microwave Limb Sounder (MLS) and WACCM-SD volcano case. MLS observations are shown for individual years from 2007 to 2021 in gray lines. The black line indicates the MLS climatological mean. The red, blue and green lines are for 2022 MLS ozone, the 2022 WACCM6-SD volcano case, and 2015 MLS ozone, respectively.

stratospheric volcanic injections from 2007 to 2021. Starting in January 2022, we run two different cases: the volcano case with forcing (SO_2 and H_2O injection) from the HTHH eruption and the control case with no forcing (no SO_2 or H_2O injection) from the HTHH eruption. The difference between these two nudged simulations gives information about the chemistry contribution to stratospheric ozone depletion after the HTHH eruption. We use the emissions described in Zhu et al. (2022), where 150 Tg of H_2O and 0.42 Tg of SO_2 are injected on 15 January 2022, from ~20 to 35 km.

3. Results and Discussions

3.1. Observed and Simulated Ozone Anomaly From MLS and WACCM6-SD

Figure 1 shows MLS observed ozone from 2007 to 2022 and WACCM6-SD simulated ozone in the volcano case during 2022. MLS satellite observations indicate anomalous negative ozone in 2022 over SH midlatitudes and tropics (10°S–60°S) in winter as well as over Antarctica (60°S–82°S) in spring. Two levels, 30 and 80 hPa, are

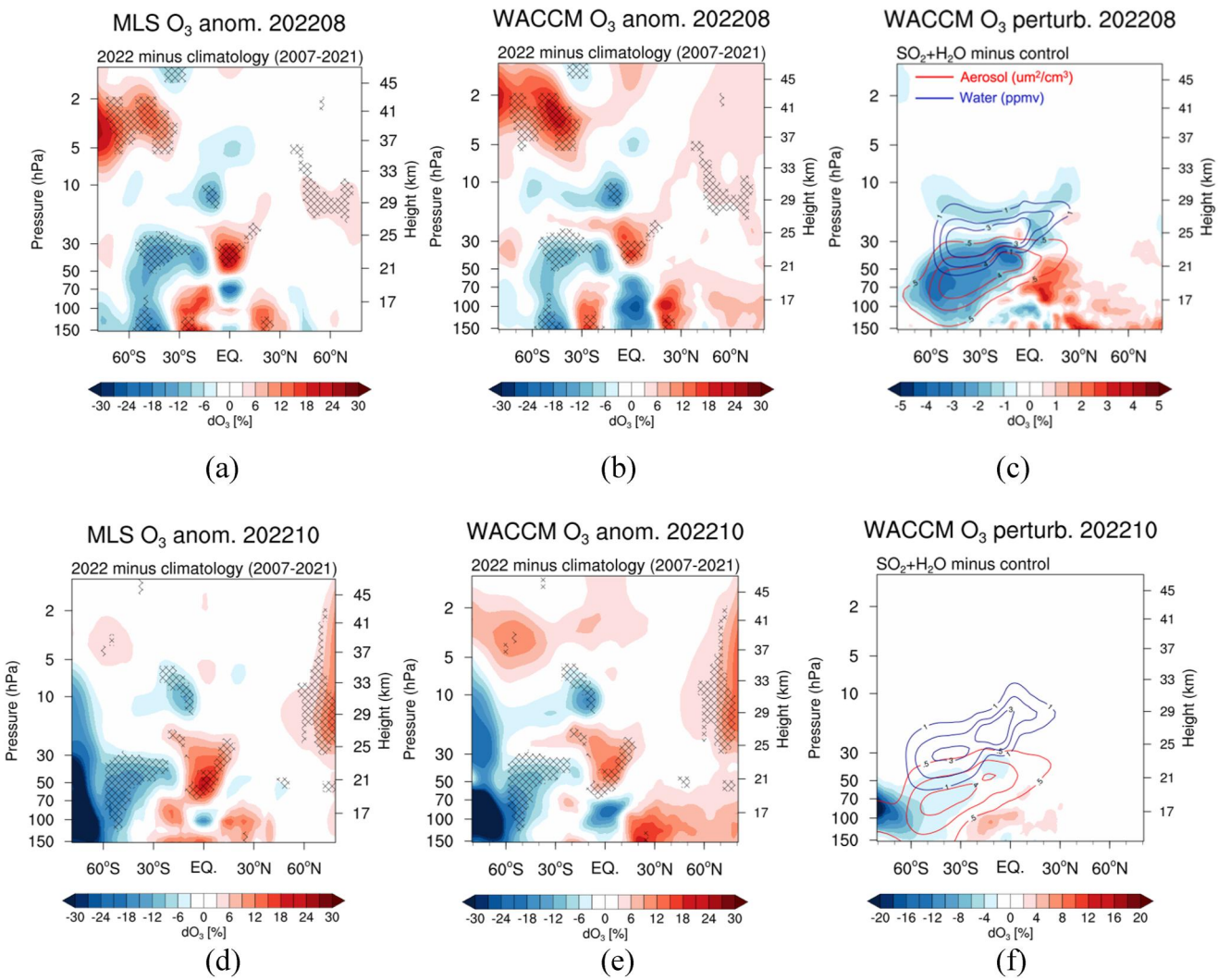

Figure 2. The 2022 ozone anomaly (%) relative to the climatology (2007–2021) from Microwave Limb Sounder (a) and WACCM6-SD volcano case (b) in August. (d, e) are the same but for October. Hatched regions indicate where the 2022 anomalies are outside the range of all variability during 2007–2021. The ozone perturbation (%) is calculated from the volcano compared to control cases in August (c) and October (f). The blue and red contour lines in panels (c, f) are the modeled water anomaly in ppmv and aerosol surface area density anomaly in $\mu m^2/cm^3$, respectively. Note that panels c and f have different color bar ranges from panels (a, b, d, e).

chosen to illustrate the cross section of the observed large negative anomalies in these latitude ranges (see below in Figures 2a and 2d). The climatology is defined as 2007 to 2021 throughout this paper to match with the model period. Anomalies for 2022 are calculated based on climatological mean. MLS ozone concentration over 10°S–60°S show a record low relative to the climatology in the SH austral winter (Figure 1a, red line) at 30 hPa. Large midwinter interannual variability in this region is linked to the phase of the Quasi-Biennial Oscillation (QBO), as discussed in Wang et al. (2023). MLS also shows a relatively deep ozone hole in the SH austral spring (Figure 1b) at 80 hPa. The negative ozone anomaly over Antarctica is large in October-December, but within the variability of previous years. This is because the climatology also includes years with either a relatively strong polar vortex or volcanic impact. For example, the lowest line (in green) in Figure 1b is in the year 2015, when a record October ozone hole occurred after the Calbuco volcanic eruption (Ivy et al., 2017; Solomon et al., 2015). The accuracy of MLS O_3 is about 0.2 ppmv at 30 hPa and 0.1 ppmv near 80 hPa (Livesey et al., 2020). The difference between MLS ozone in 2022 and the climatological mean is outside the MLS systematic error during June-August and October, which reinforces the idea that the anomalous low ozone occurring in the SH mid-latitudes winter and Antarctica spring 2022 is due to HTHH. WACCM6-SD captures both the record low ozone over 10°S–60°S and the large ozone anomaly over 60°S–82°S, and is within the systematic error of MLS.

3.2. Chemistry Contribution to the Stratospheric Ozone Depletion

Both the observed and simulated 2022 anomalies shown in Figure 2 are calculated as deviations from the climatological mean, which includes a mix of QBO phases. Thus, the derived stratospheric ozone anomaly consists of both the influence of the 2022 QBO phase and the forced changes after the HTHH eruption, including both dynamical and chemical impacts. The 2022 anomalies from MLS and WACCM6-SD in August are shown in Figures 2a and 2b. The lower stratospheric SH mid-latitude ozone reduction is well represented in WACCM6-SD. Figure 2c shows the ozone changes due to chemistry only, calculated by taking the difference between the volcano case and the control case in 2022. The blue and red contour lines highlight the location of HTHH water and aerosol plumes, which reveals the separation of the H_2O and aerosol plumes over time due to the sedimentation of the aerosols (Legras et al., 2022; Wang et al., 2023). As the volcano and control simulations are nudged to the same dynamics, the ozone changes in Figure 2c are primarily due to the chemistry impact from the enhanced water and the aerosol SAD perturbations. The ozone reduction at 30 to 50 hPa over the SH mid-latitudes are outside of previous variability (hatched region in Figures 2a and 2b). The maximum ozone reduction reaches about 15% in the hatched region (Figure 2a), which is the combination of dynamical and chemical influences. Chemistry yields 4% ozone loss at mid-latitudes near ∼70 hPa in August (Figure 2c). The majority of the ozone reduction is a result of dynamical changes due to internal variability from the QBO and a forced dynamical response from the HTHH eruption.

In the Antarctic, a large negative ozone anomaly is observed within the polar vortex in October 2022 (Figure 2d), even though there is not a record-breaking low ozone hole (not hatched). WACCM6-SD reproduces this large ozone reduction in general, but slightly underestimates the ozone depletion between 30 and 50 hPa (Figure 2e). The simulated perturbation due to HTHH (Figure 2f) shows that the aerosol plume entered the Antarctic near the bottom of the polar vortex (∼100 hPa) in October. However, in 2022 the water plume was confined outside of the polar vortex due to the strong polar jet stream near 25 km (Manney et al., 2023; Schoeberl et al., 2022). Note that although the simulated HTHH aerosol distribution penetrated across the bottom of the polar vortex, this feature is difficult to validate with available observations. For example, enhanced polar extinction in OMPS-LP measurements could be due to polar stratospheric clouds in winter (Manney et al., 2023; Wang et al., 2023). In addition, the amount of sulfate entering the polar vortex in the simulation is relatively small, and satellite observation (e.g., CALIPSO lidar) is not able to capture it due to background noise level. The ozone depletion simulated in Figure 2f occurs because the volcanic aerosol entered the bottom of the polar vortex, which provides additional SAD for heterogeneous chemistry in the polar region. The chemical impact of the simulated HTHH perturbations (Figure 2f) leads to ∼20% ozone loss near the center of the Antarctic vortex at 80 hPa in October.

Odd oxygen destruction (see definition in Text S1 in Supporting Information S1 which is taken from Brasseur & Solomon, 2005) is directly linked to ozone abundance in the stratosphere. Different odd oxygen catalytic destruction cycles involve nitrogen oxides (NO_x cycle), hydrogen radicals (HO_x cycle), halogen oxides (ClO_x/BrO_x cycle) and Chapman self-destruction incorporating $O(^1D) + H_2O$ (O_x cycle) (e.g., Crutzen & Ehhalt, 1977; Solomon, 1999). Text S1 in Supporting Information S1 defines the odd oxygen chemistry used in this study and the reactions that are contained in each odd oxygen chemical family. Figures 3a and 3b characterize the changes in total odd oxygen loss (sum of O_x, NO_x, HO_x and ClO_x/BrO_x cycles) in the SH during August and October. In August, the major odd oxygen loss occurs in the mid-latitudes from 150 to 20 hPa, consistent with the location of major ozone loss in Figure 2c. In October, the total odd oxygen loss extends into the polar region, associated with the aerosol plume shown in Figure 2f.

Vertical profile of changes in individual loss cycles are illustrated in Figures 3c and 3d for mid-latitudes in August and Antarctic in October, respectively. Increasing aerosol surface areas decreases the abundance of NO_x, which decreases the amount of ozone loss from the NO_x cycle (discussed in Section 3.3 below). The enhanced HO_x cycle is the combined result of direct water injection and HO_x repartitioning induced by the NO_x reduction (Solomon et al., 1996; Wennberg et al., 1994). The reduced NO_x also gives rise to ClO_x enhancements as ClO_x is inversely correlated with NO_x (Stimpfle et al., 1994; Solomon, 1999). In the Antarctic spring, the ClO_x/BrO_x cycle controls the behavior of odd oxygen change below 70 hPa. The HO_x cycle is the major loss mechanism at 70–30 hPa. However, this loss is largely offset by hindered NOx cycle, which is normally the most important loss cycle at this altitude in the background atmosphere (Zhang et al., 2021). It is noticeable there is a negative odd oxygen perturbation at around 70–100 hPa in Figures 3b and 3d. This is because the ozone abundances in the volcano case drop to extreme low values at 70-100 hPa in the core of the vortex, so the formation of ClO (and therefore chlorine

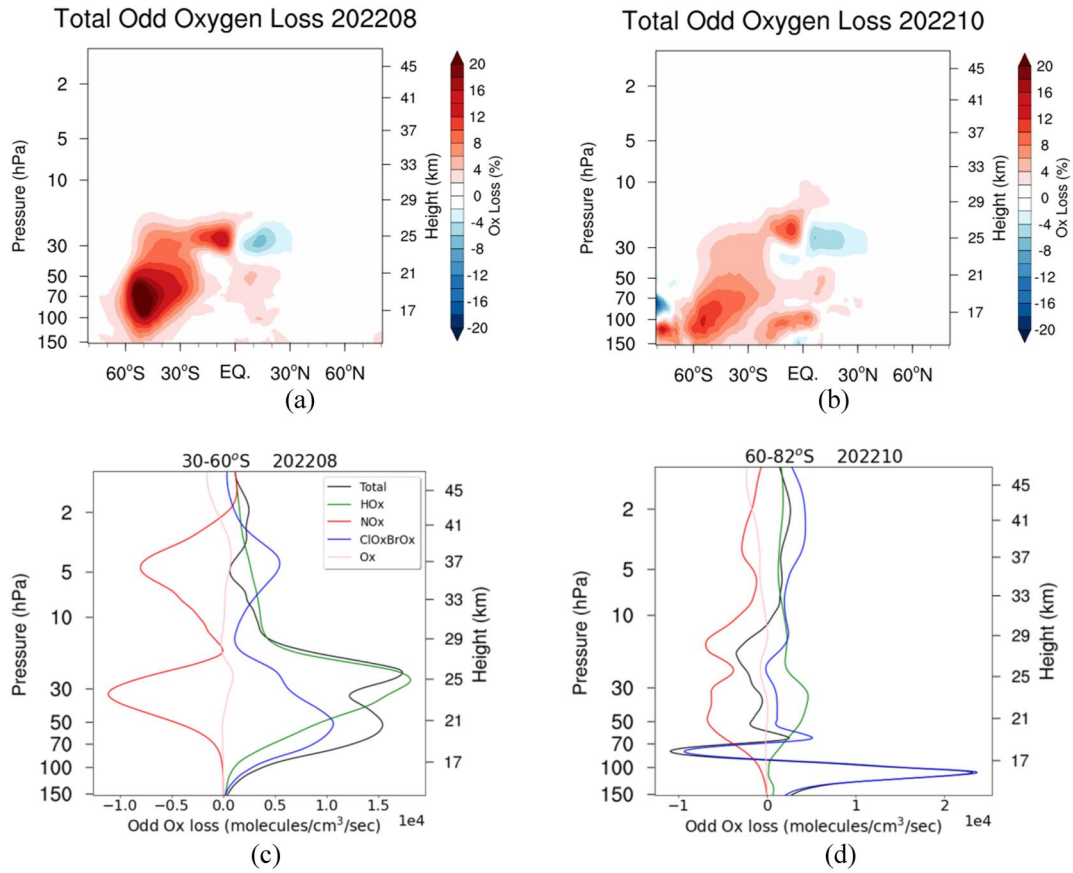

Figure 3. Calculated perturbations from the volcano case compared to control case for total odd oxygen loss in August (a) and October (b). Vertical profiles of changes in total odd oxygen loss (black line) and the loss from HO_x, NO_x, ClO_xBrO_x and O_x cycles at mid-latitudes in August (c) and the Antarctic in October (d).

nitrate ($ClONO_2$) is impeded (Figure S2 in Supporting Information S1). Rapid deactivation of Cl into hydrochloric acid (HCl) then occurs even if the enhanced SAD is still present and temperatures are very cold (Douglass et al., 1995; Solomon et al., 2015). This rapid deactivation suppresses the odd oxygen loss due to the ClO_x/BrO_x cycle in the volcano case compared to the control case.

3.3. NO_x and Nitric Acid (HNO_3) Anomalies After HTHH Eruption

NO_x reduction and HNO_3 increase is expected following large volcanic eruptions, which perturb ozone abundances in the stratosphere (e.g., Fahey et al., 1993; Mills et al., 1993; Zambri et al., 2019). Figure 4 examines the NO_x and HNO_3 anomaly after the HTHH eruption from OSIRIS and MLS observations, along with WACCM6-SD simulations. A dipole NO_x pattern is observed both in OSIRIS and WACCM where there is a NO_x reduction around 25 km and below, and a positive anomaly above. This positive anomaly is mainly due to the QBO induced internal variability, as it is also seen in 2008 when the QBO phase is similar to the phase in 2022 (Park et al., 2017). The negative NO_x anomaly is not normally present (Figure S3 in Supporting Information S1). Both the observations and model show a negative NO_x anomaly in August 2022 (Figures 4a and 4b), with reductions of 40%–50% over the mid-latitude lower stratosphere. This negative anomaly is approximately co-located with the HTHH aerosol plume in Figure 4b in red contour lines. The HTHH aerosol reduces the NO_x abundance via the well-known heterogeneous chemical reaction of dinitrogen pentoxide (N_2O_5) hydrolysis on aerosols, along with an increase in HNO_3 (e.g., Berthet et al., 2017; Hofmann & Solomon, 1989). Due to the N_2O_5 hydrolysis on the surface of aerosols, HNO_3 formation is promoted which acts as a major sink of NO_x in the atmosphere during night-time. Model calculations (Figure 4b) show similar NO_x decreases in the lower stratosphere to the OSIRIS results, demonstrating that the NO_x-aerosol reactions are captured well in the model. We note that OSIRIS does not have high latitude measurements during midwinter. Figure 4c shows the modeled NO_x perturbation, derived

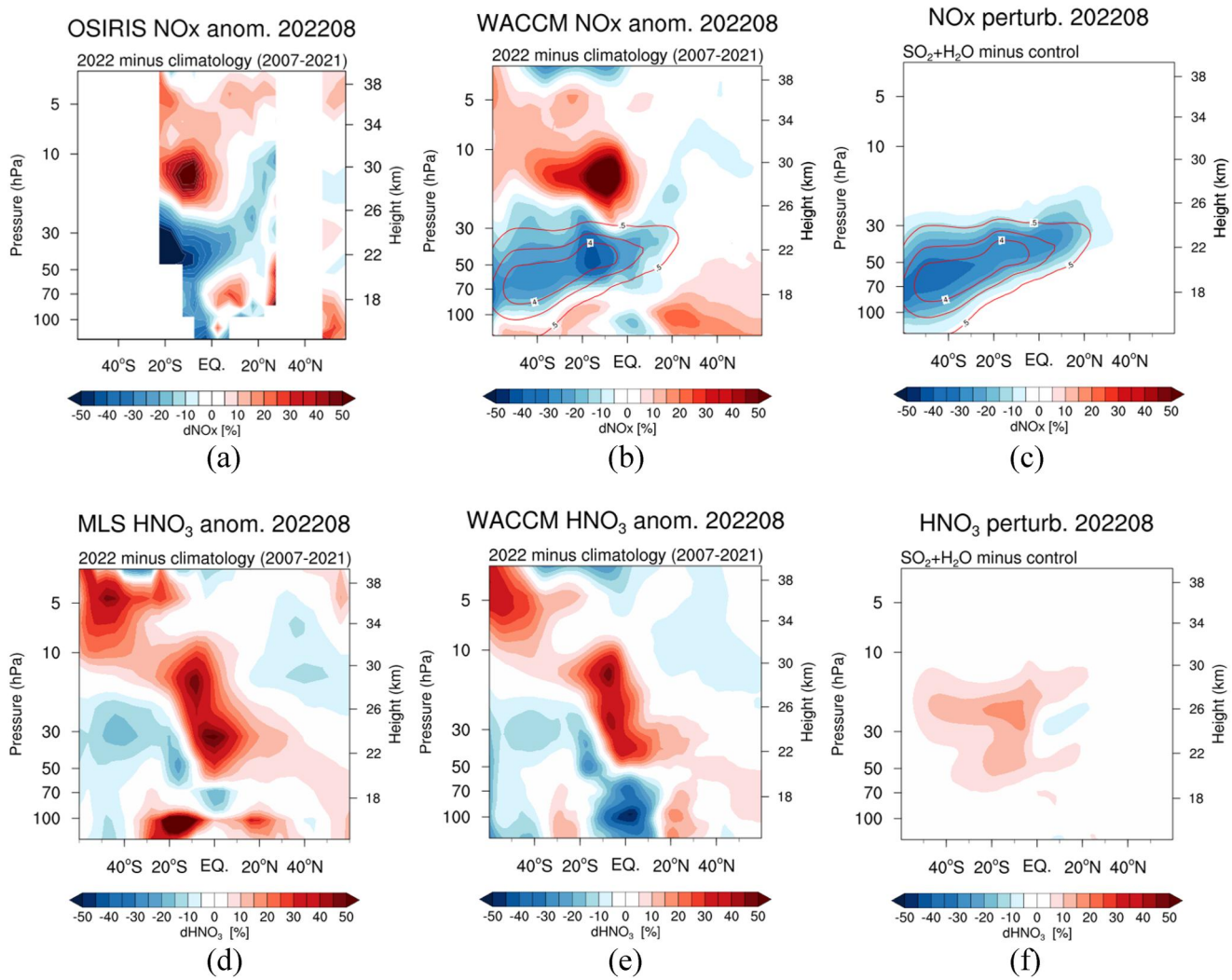

Figure 4. Calculated NO_x anomaly (%) relative to climatology (2007–2021) from OSIRIS (a) and WACCM6-SD (b) in August. (c) is the NO_x perturbation in the WACCM6-SD from the volcano case compared to the control case in August. (d, e) are HNO_3 anomaly relative to climatology from Microwave Limb Sounder and WACCM6-SD in August. (f) is the HNO_3 perturbation. The red contour lines in panels (b, c) are the modeled aerosol surface area density anomaly in $\mu m^2/cm^3$.

from the difference between volcano and control cases, overlying the aerosol SAD anomaly due to the HTHH eruption. This NO_x reduction is the result of N_2O_5 hydrolysis being enhanced by up to 40% (Figure S4 in Supporting Information S1). The decrease in the abundance of NO_x is accompanied by a corresponding increase in HNO_3 (Figure 4f) from the N_2O_5 hydrolysis. However, this chemical signal is obscured by dynamical variability, where a negative anomaly (10%–20%) in the SH mid-latitudes between 20 and 50 hPa were found in both the observed and modeled HNO_3 anomalies versus climatology (Figures 4d and 4e). The results shown here are consistent with the conclusion drawn from Santee et al. (2023) using MLS data, suggesting that hydrolysis of N_2O_5 is the primary mechanism for the reduction of NO_x, along with enhancement of HNO_3. We note that even though this NO_x reduction is significant, we found that the NO_x impact on ozone is largely canceled by the HO_x and ClO_x cycles as shown in Figures 3c and 3d.

4. Summary and Discussion

This work focused on examining the chemical ozone depletion due to the SO_2 and H_2O injections from the HTHH eruption. We used WACCM6-SD nudged simulations to disentangle the role of chemistry from that of dynamics. WACCM6-SD shows a good agreement with MLS ozone and HNO_3 anomalies and also reproduces the NO_x anomaly observed by OSIRIS.

We found chemistry yields about 4% ozone loss at mid-latitudes near ~70 hPa in August and 20% ozone loss over Antarctica near ~80 hPa in October. Most of the ozone changes relative to the 2007–2021 climatology are due to transport and dynamical processes from internal variability in the climate system, along with the forced response from the HTHH eruption. One caveat is that the chemistry examined here does not include the dynamical feedback on the chemistry. For example, water can cool the stratosphere, which would further promote heterogeneous reactions. However, because the two simulations conducted here are nudged to the same dynamics, the temperature is not allowed to adjust to reflect the feedback on chemistry. Different odd-oxygen loss cycles (NO_x, HO_x, ClO_x/BrO_x and O_x cycles) were examined and their relative significance to the ozone depletion at SH mid-latitudes and Antarctica were evaluated. We found both HO_x and ClO_x/BrO_x cycles play important roles in the total chemical ozone destruction for mid-latitudes in August. During the Antarctic October, the ClO_x/BrO_x cycle is dominant and controls the behavior of total odd oxygen change in the lower stratosphere. We also find that both OSIRIS and WACCM6-SD show a NO_x reduction that co-locates with the HTHH aerosol plume, demonstrating the enhanced N_2O_5 hydrolysis rate on sulfate aerosol. Consequently, the NO_x odd-oxygen loss cycle is strongly suppressed. However, the NO_x impact on ozone is minimal since it is largely canceled by the increase in the HO_x and ClO_x/BrO_x cycles.

Data Availability Statement

CESM2/WACCM6 (described in Gettelman et al., 2019) is an open-source community model, which was developed with support primarily from the National Science Foundation. Figures in this study are plotted using the NCAR Command Language (Version 6.6.2) (The NCAR Command Language, 2019). The atmospheric modeling data set used in the analysis is published (Zhang et al., 2023).

Acknowledgments

Jun Zhang and Xinyue Wang are supported by the NSF via NCAR's Advanced Study Program Postdoctoral Fellowship. Douglas Kinnison is partially supported by NASA Grant 80NSSC19K0952. NCAR's Community Earth System Model project is supported primarily by the National Science Foundation. This material is based upon work supported by the National Center for Atmospheric Research, which is a major facility sponsored by the NSF under Cooperative Agreement No. 1852977. Computing and data storage resources, including the Cheyenne supercomputer (doi: 10.5065/D6RX99HX), were provided by the Computational and Information Systems Laboratory (CISL) at NCAR. The authors thank the Swedish National Space Agency and the Canadian Space Agency for the continued operation and support of Odin-OSIRIS. Kimberlee Dube is supported by the Canadian Space Agency (Grant 21SUASULSO). This project received funding from NOAA's Earth Radiation Budget (ERB) Initiative (CPO #03-01-07-001). Yunqian Zhu is supported in part by NOAA cooperative agreements NA17OAR4320101 and NA22OAR4320151.

References

Anderson, J. G., Wilmouth, D. M., Smith, J. B., & Sayres, D. S. (2012). UV dosage levels in summer: Increased risk of ozone loss from convectively injected water vapor. *Science*, *337*(6096), 835–839. https://doi.org/10.1126/science.1222978

Berthet, G., Jégou, F., Catoire, V., Krysztofiak, G., Renard, J. B., Bourassa, A. E., et al. (2017). Impact of a moderate volcanic eruption on chemistry in the lower stratosphere: Balloon-borne observations and model calculations. *Atmospheric Chemistry and Physics*, *17*(3), 2229–2253. https://doi.org/10.5194/acp-17-2229-2017

Bourassa, A. E., Zawada, D. J., Rieger, L. A., Warnock, T. W., Toohey, M., & Degenstein, D. A. (2023). Tomographic retrievals of Hunga Tonga-Hunga Ha'apai volcanic aerosol. *Geophysical Research Letters*, *50*(3), e2022GL101978. https://doi.org/10.1029/2022GL101978

Brasseur, G. P., & Solomon, S. (2005). *Aeronomy of the middle atmosphere: Chemistry and physics of the stratosphere and mesosphere* (Vol. 32). Springer Science & Business Media.

Carn, S. A., Krotkov, N. A., Fisher, B. L., & Li, C. (2022). Out of the blue: Volcanic SO2 emissions during the 2021–2022 eruptions of Hunga Tonga—Hunga Ha'apai (Tonga). *Frontiers in Earth Science*, *10*, 976962. https://doi.org/10.3389/feart.2022.976962

Carr, J. L., Horváth, Á., Wu, D. L., & Friberg, M. D. (2022). Stereo plume height and motion retrievals for the record-setting Hunga Tonga-Hunga Ha'apai eruption of 15 January 2022. *Geophysical Research Letters*, *49*(9), e2022GL098131. https://doi.org/10.1029/2022GL098131

Crutzen, P. J., & Ehhalt, D. H. (1977). Effects of nitrogen fertilizers and combustion on the stratospheric ozone layer. *Ambio*, 112–117. Retrieved from https://www.jstor.org/stable/4312257

Davis, N. A., Callaghan, P., Simpson, I. R., & Tilmes, S. (2022). Specified dynamics scheme impacts on wave-mean flow dynamics, convection, and tracer transport in CESM2 (WACCM6). *Atmospheric Chemistry and Physics*, *22*(1), 197–214. https://doi.org/10.5194/acp-22-197-2022

Douglass, A. R., Schoeberl, M. R., Stolarski, R. S., Waters, J. W., Russell III, J. M., Roche, A. E., & Massie, S. T. (1995). Interhemispheric differences in springtime production of HCl and $ClONO_2$ in the polar vortices. *Journal of Geophysical Research*, *100*(D7), 13967–13978. https://doi.org/10.1029/95JD00698

Dubé, K., Randel, W., Bourassa, A., Zawada, D., McLinden, C., & Degenstein, D. (2020). Trends and variability in stratospheric NOx derived from merged SAGE II and OSIRIS satellite observations. *Journal of Geophysical Research: Atmospheres*, *125*(7), e2019JD031798. https://doi.org/10.1029/2019JD031798

Dubé, K., Zawada, D., Bourassa, A., Degenstein, D., Randel, W., Flittner, D., et al. (2022). An improved OSIRIS NO2 profile retrieval in the upper troposphere–lower stratosphere and intercomparison with ACE-FTS and SAGE III/ISS. *Atmospheric Measurement Techniques*, *15*(20), 6163–6180. https://doi.org/10.5194/amt-15-6163-2022

Fahey, D. W., Kawa, S. R., Woodbridge, E. L., Tin, P., Wilson, J. C., Jonsson, H. H., et al. (1993). In situ measurements constraining the role of sulphate aerosols in mid-latitude ozone depletion. *Nature*, *363*(6429), 509–514. https://doi.org/10.1038/363509a0

Gelaro, R., McCarty, W., Suárez, M. J., Todling, R., Molod, A., Takacs, L., et al. (2017). The modern-era retrospective analysis for research and applications, version 2 (MERRA-2). *Journal of Climate*, *30*(14), 5419–5454. https://doi.org/10.1175/JCLI-D-16-0758.1

Gettelman, A., Mills, M. J., Kinnison, D. E., Garcia, R. R., Smith, A. K., Marsh, D. R., et al. (2019). The whole atmosphere community climate model version 6 (WACCM6). *Journal of Geophysical Research: Atmospheres*, *124*(23), 12380–12403. https://doi.org/10.1029/2019JD030943

Hofmann, D. J., & Solomon, S. (1989). Ozone destruction through heterogeneous chemistry following the eruption of El Chichon. *Journal of Geophysical Research*, *94*(D4), 5029–5041. https://doi.org/10.1029/JD094iD04p05029

Ivy, D. J., Solomon, S., Kinnison, D., Mills, M. J., Schmidt, A., & Neely III, R. R. (2017). The influence of the Calbuco eruption on the 2015 Antarctic ozone hole in a fully coupled chemistry-climate model. *Geophysical Research Letters*, *44*(5), 2556–2561. https://doi.org/10.1002/2016GL071925

Khaykin, S., Podglajen, A., Ploeger, F., Grooß, J. U., Tencé, F., Bekki, S., et al. (2022). Global perturbation of stratospheric water and aerosol burden by Hunga eruption. *Communications Earth & Environment*, *3*(1), 316. https://doi.org/10.1038/s43247-022-00652-x

Kinnison, D. E., Grant, K. E., Connell, P. S., Rotman, D. A., & Wuebbles, D. J. (1994). The chemical and radiative effects of the Mount Pinatubo eruption. *Journal of Geophysical Research*, *99*(D12), 25705–25731. https://doi.org/10.1029/94JD02318

Kloss, C., Sellitto, P., Renard, J. B., Baron, A., Bègue, N., Legras, B., et al. (2022). Aerosol characterization of the stratospheric plume from the volcanic eruption at Hunga Tonga 15 January 2022. *Geophysical Research Letters*, *49*(16), e2022GL099394. https://doi.org/10.1029/2022GL099394

Krueger, A. J., Walter, L. S., Bhartia, P. K., Schnetzler, C. C., Krotkov, N. A., Sprod, I. T., & Bluth, G. J. S. (1995). Volcanic sulfur dioxide measurements from the total ozone mapping spectrometer instruments. *Journal of Geophysical Research*, *100*(D7), 14057–14076. https://doi.org/10.1029/98GL00178

Legras, B., Duchamp, C., Sellitto, P., Podglajen, A., Carboni, E., Siddans, R., et al. (2022). The evolution and dynamics of the Hunga Tonga–Hunga Ha'apai sulfate aerosol plume in the stratosphere. *Atmospheric Chemistry and Physics*, *22*(22), 14957–14970. https://doi.org/10.5194/acp-22-14957-2022

Lin, S. J., & Rood, R. B. (1996). Multidimensional flux-form semi-Lagrangian transport schemes. *Monthly Weather Review*, *124*(9), 2046–2070. https://doi.org/10.1175/1520-0493(1996)124<2046:MFFSLT>2.0.CO;2

Livesey, N. J., Read, W. G., Wagner, P. A., Froidevaux, L., Santee, M. L., & Schwartz, M. J. (2020). *Version 5.0 x level 2 and 3 data quality and description document* (Tech. Rep. No. JPL D-105336 Rev. A). Jet Propulsion Laboratory.

Llewellyn, E. J., Lloyd, N. D., Degenstein, D. A., Gattinger, R. L., Petelina, S. V., Bourassa, A. E., et al. (2004). The OSIRIS instrument on the Odin spacecraft. *Canadian Journal of Physics*, *82*(6), 411–422. https://doi.org/10.1139/p04-005

Lu, J., Lou, S., Huang, X., Xue, L., Ding, K., Liu, T., et al. (2023). Stratospheric aerosol and ozone responses to the Hunga Tonga-Hunga Ha'apai volcanic eruption. *Geophysical Research Letters*, *50*(4), e2022GL102315. https://doi.org/10.1029/2022GL102315

Manney, G. L., Santee, M. L., Lambert, A., Millán, L. F., Minschwaner, K., Werner, F., et al. (2023). Siege in the southern stratosphere: Hunga Tonga-Hunga Ha'apai water vapor excluded from the 2022 Antarctic polar vortex. *Geophysical Research Letters*, *50*(14), e2023GL103855. https://doi.org/10.1029/2023GL103855

McLinden, C. A., Olsen, S. C., Hannegan, B., Wild, O., Prather, M. J., & Sundet, J. (2000). Stratospheric ozone in 3-D models: A simple chemistry and the cross-tropopause flux. *Journal of Geophysical Research*, *105*(D11), 14653–14665. https://doi.org/10.1029/2000JD900124

Millan, L., Santee, M. L., Lambert, A., Livesey, N. J., Werner, F., Schwartz, M. J., et al. (2022). The Hunga Tonga-Hunga Ha'apai hydration of the stratosphere. *Geophysical Research Letters*, *49*(13), e2022GL099381. https://doi.org/10.1029/2022GL099381

Mills, M. J., Langford, A. O., O'Leary, T. J., Arpag, K., Miller, H. L., Proffitt, M. H., et al. (1993). On the relationship between stratospheric aerosols and nitrogen dioxide. *Geophysical Research Letters*, *20*(12), 1187–1190. https://doi.org/10.1029/93GL01124

Mills, M. J., Richter, J. H., Tilmes, S., Kravitz, B., MacMartin, D. G., Glanville, A. A., et al. (2017). Radiative and chemical response to interactive stratospheric sulfate aerosols in fully coupled CESM1 (WACCM). *Journal of Geophysical Research: Atmospheres*, *122*(23), 13–061. https://doi.org/10.1002/2017JD027006

Mills, M. J., Schmidt, A., Easter, R., Solomon, S., Kinnison, D. E., Ghan, S. J., et al. (2016). Global volcanic aerosol properties derived from emissions, 1990–2014, using CESM1 (WACCM). *Journal of Geophysical Research: Atmospheres*, *121*(5), 2332–2348. https://doi.org/10.1002/2015JD024290

Murtagh, D., Frisk, U., Merino, F., Ridal, M., Jonsson, A., Stegman, J., et al. (2002). An overview of the Odin atmospheric mission. *Canadian Journal of Physics*, *80*(4), 309–319. https://doi.org/10.1139/p01-157

Park, M., Randel, W. J., Kinnison, D. E., Bourassa, A. E., Degenstein, D. A., Roth, C. Z., et al. (2017). Variability of stratospheric reactive nitrogen and ozone related to the QBO. *Journal of Geophysical Research: Atmospheres*, *122*(18), 10–103. https://doi.org/10.1002/2017JD027061

Portmann, R. W., Solomon, S., Garcia, R. R., Thomason, L. W., Poole, L. R., & McCormick, M. P. (1996). Role of aerosol variations in anthropogenic ozone depletion in the polar regions. *Journal of Geophysical Research*, *101*(D17), 22991–23006. https://doi.org/10.1029/96JD02608

Prather, M., & Jaffe, A. H. (1990). Global impact of the Antarctic ozone hole: Chemical propagation. *Journal of Geophysical Research*, *95*(D4), 3473–3492. https://doi.org/10.1029/JD095iD04p03473

Proud, S. R., Prata, A. T., & Schmauß, S. (2022). The January 2022 eruption of Hunga Tonga-Hunga Ha'apai volcano reached the mesosphere. *Science*, *378*(6619), 554–557. https://doi.org/10.1126/science.abo4076

Randel, W. J., Johnston, B. R., Braun, J. J., Sokolovskiy, S., Vömel, H., Podglajen, A., & Legras, B. (2023). Stratospheric water vapor from the Hunga Tonga–Hunga Ha'apai volcanic eruption deduced from COSMIC-2 radio occultation. *Remote Sensing*, *15*(8), 2167. https://doi.org/10.3390/rs15082167

Read, W. G., Froidevaux, L., & Waters, J. W. (1993). Microwave limb sounder measurement of stratospheric SO2 from the Mt. Pinatubo Volcano. *Geophysical Research Letters*, *20*(12), 1299–1302. https://doi.org/10.1029/93GL00831

Santee, M. L., Lambert, A., Froidevaux, L., Manney, G. L., Schwartz, M. J., Millán, L. F., et al. (2023). Strong evidence of heterogeneous processing on stratospheric sulfate aerosol in the extrapolar Southern Hemisphere following the 2022 Hunga Tonga-Hunga Ha'apai eruption. *Journal of Geophysical Research: Atmospheres*, *128*(16), e2023JD039169. https://doi.org/10.1029/2023JD039169

Schoeberl, M. R., Wang, Y., Ueyama, R., Taha, G., Jensen, E., & Yu, W. (2022). Analysis and impact of the Hunga Tonga-Hunga Ha'apai stratospheric water vapor plume. *Geophysical Research Letters*, *49*(20), e2022GL100248. https://doi.org/10.1029/2022GL100248

Solomon, S. (1999). Stratospheric ozone depletion: A review of concepts and history. *Reviews of Geophysics*, *37*(3), 275–316. https://doi.org/10.1029/1999RG900008

Solomon, S., Borrmann, S., Garcia, R. R., Portmann, R., Thomason, L., Poole, L. R., et al. (1997). Heterogeneous chlorine chemistry in the tropopause region. *Journal of Geophysical Research*, *102*(D17), 21411–21429. https://doi.org/10.1029/97JD01525

Solomon, S., Ivy, D. J., Kinnison, D., Mills, M. J., Neely III, R. R., & Schmidt, A. (2016). Emergence of healing in the Antarctic ozone layer. *Science*, *353*(6296), 269–274. https://doi.org/10.1126/science.aae0061

Solomon, S., Kinnison, D., Bandoro, J., & Garcia, R. (2015). Simulation of polar ozone depletion: An update. *Journal of Geophysical Research: Atmospheres*, *120*(15), 7958–7974. https://doi.org/10.1002/2015JD023365

Solomon, S., Portmann, R. W., Garcia, R. R., Randel, W., Wu, F., Nagatani, R., et al. (1998). Ozone depletion at mid-latitudes: Coupling of volcanic aerosols and temperature variability to anthropogenic chlorine. *Geophysical Research Letters*, *25*(11), 1871–1874. https://doi.org/10.1029/98GL01293

Solomon, S., Portmann, R. W., Garcia, R. R., Thomason, L. W., Poole, L. R., & McCormick, M. P. (1996). The role of aerosol variations in anthropogenic ozone depletion at northern midlatitudes. *Journal of Geophysical Research*, *101*(D3), 6713–6727. https://doi.org/10.1029/95JD03353

Solomon, S., Portmann, R. W., Sasaki, T., Hofmann, D. J., & Thompson, D. W. (2005). Four decades of ozonesonde measurements over Antarctica. *Journal of Geophysical Research*, *110*(D21). https://doi.org/10.1029/2005JD005917

Stimpfle, R. M., Koplow, J. P., Cohen, R. C., Kohn, D. W., Wennberg, P. O., Judah, D. M., et al. (1994). The response of ClO radical concentrations to variations in NO2 radical concentrations in the lower stratosphere. *Geophysical Research Letters*, *21*(23), 2543–2546. https://doi.org/10.1029/94GL02373

Stone, K. A., Solomon, S., Kinnison, D. E., Pitts, M. C., Poole, L. R., Mills, M. J., et al. (2017). Observing the impact of Calbuco volcanic aerosols on South Polar ozone depletion in 2015. *Journal of Geophysical Research: Atmospheres*, *122*(21), 11–862. https://doi.org/10.1002/2017JD026987

Taha, G., Loughman, R., Colarco, P. R., Zhu, T., Thomason, L. W., & Jaross, G. (2022). Tracking the 2022 Hunga Tonga-Hunga Ha'apai aerosol cloud in the upper and middle stratosphere using space-based observations. *Geophysical Research Letters*, *49*(19), e2022GL100091. https://doi.org/10.1029/2022GL100091

The NCAR Command Language. (2019). UCAR/NCAR/CISL/TDD (version 6.6.2) [Software]. https://doi.org/10.5065/D6WD3XH5

Tie, X., & Brasseur, G. (1995). The response of stratospheric ozone to volcanic eruptions: Sensitivity to atmospheric chlorine loading. *Geophysical Research Letters*, *22*(22), 3035–3038. https://doi.org/10.1029/95GL03057

Vömel, H., Evan, S., & Tully, M. (2022). Water vapor injection into the stratosphere by Hunga Tonga-Hunga Ha'apai. *Science*, *377*(6613), 1444–1447. https://doi.org/10.1126/science.abq2299

Wang, X., Randel, W., Zhu, Y., Tilmes, S., Starr, J., Yu, W., et al. (2023). Stratospheric climate anomalies and ozone loss caused by the Hunga Tonga-Hunga Ha'apai volcanic eruption. *Journal of Geophysical Research: Atmospheres*, *128*(22), e2023JD039480. https://doi.org/10.1029/2023JD039480

Wennberg, P. O., Cohen, R. C., Stimpfle, R. M., Koplow, J. P., Anderson, J. G., Salawitch, R. J., et al. (1994). Removal of stratospheric O_3 by radicals: In situ measurements of OH, HO_2, NO, NO_2, ClO, and BrO. *Science*, *266*(5184), 398–404. https://doi.org/10.1126/science.266.5184.398

Zambri, B., Solomon, S., Kinnison, D. E., Mills, M. J., Schmidt, A., Neely III, R. R., et al. (2019). Modeled and observed volcanic aerosol control on stratospheric NOy and Cly. *Journal of Geophysical Research: Atmospheres*, *124*(17–18), 10283–10303. https://doi.org/10.1029/2019JD031111

Zhang, J., Kinnison, D., Zhu, Y., Wang, X., Tilmes, S., Dube, K., & Randel, W. (2023). UCAR/NCAR - GDEX (version 1.0.) [Dataset]. https://doi.org/10.5065/nsar-fh76

Zhang, J., Wuebbles, D., Kinnison, D., & Baughcum, S. L. (2021). Stratospheric ozone and climate forcing sensitivity to cruise altitudes for fleets of potential supersonic transport aircraft. *Journal of Geophysical Research: Atmospheres*, *126*(16), e2021JD034971. https://doi.org/10.1029/2021JD034971

Zhu, Y., Bardeen, C. G., Tilmes, S., Mills, M. J., Wang, X., Harvey, V. L., et al. (2022). Perturbations in stratospheric aerosol evolution due to the water-rich plume of the 2022 Hunga-Tonga eruption. *Communications Earth & Environment*, *3*(1), 248. https://doi.org/10.1038/s43247-022-00580-w

Zhu, Y., Toon, O. B., Kinnison, D., Harvey, V. L., Mills, M. J., Bardeen, C. G., et al. (2018). Stratospheric aerosols, polar stratospheric clouds, and polar ozone depletion after the Mount Calbuco eruption in 2015. *Journal of Geophysical Research: Atmospheres*, *123*(21), 12–308. https://doi.org/10.1029/2018JD028974